A computational and experimental study of the linear and nonlinear response of a star polymer melt with a moderate number of unentangled arms

Barry W. Fitzgerald, Helen Lentzakis, Georgios Sakellariou, Dimitris Vlassopoulos, and Wim J. Briels

Citation: The Journal of Chemical Physics **141**, 114907 (2014); doi: 10.1063/1.4895610
View online: http://dx.doi.org/10.1063/1.4895610
View Table of Contents: http://scitation.aip.org/content/aip/journal/jcp/141/11?ver=pdfcov
Published by the AIP Publishing

A computational and experimental study of the linear and nonlinear response of a star polymer melt with a moderate number of unentangled arms

Barry W. Fitzgerald,[1,a)] Helen Lentzakis,[2,3] Georgios Sakellariou,[4] Dimitris Vlassopoulos,[2,3] and Wim J. Briels[1]
[1]*Computational Biophysics, University of Twente, P.O. Box 217, 7500 AE, Enschede, The Netherlands*
[2]*Foundation for Research and Technology (FORTH), Institute of Electronic Structure and Laser, Heraklion 71110, Crete, Greece*
[3]*University of Crete, Department of Materials Science and Technology, Heraklion 71003, Crete Greece*
[4] *Department of Chemistry, University of Athens, Athens 15771, Greece*

(Received 27 June 2014; accepted 2 September 2014; published online 17 September 2014)

We present from simulations and experiments results on the linear and nonlinear rheology of a moderate functionality, low molecular weight unentangled polystyrene (PS) star melt. The PS samples were anionically synthesized and close to monodisperse while their moderate functionality ensures that they do not display a pronounced core effect. We employ a highly coarse-grained model known as Responsive Particle Dynamics where each star polymer is approximated as a point particle. The eliminated degrees of freedom are used in the definition of an appropriate free energy as well as describing the transient pair-wise potential between particles that accounts for the viscoelastic response. First we reproduce very satisfactorily the experimental moduli using simulation. We then consider the nonlinear response of the same polymer melts by implementing a start-up shear protocol for a wide range of shear rates. As in experiments, we observe the development of a stress overshoot with increasing shear rate followed by a steady-state shear stress. We also recover the shear-thinning nature of the melt, although we slightly overestimate the extent of shear-thinning with simulations. In addition, we study relaxations upon the removal of shear where we find encouraging agreement between experiments and simulations, a finding that corroborates our agreement for the linear rheology.
 [http://dx.doi.org/10.1063/1.4895610]

I. INTRODUCTION

Complex entangled branched polymers have been the subject of increased research because of their modern industrial significance.[1] There are many variants of branched polymers including star polymers,[2] H polymers,[3] and combs.[4] Star polymers, which are the simplest branched polymers, represent an interesting form of soft matter in that their behaviours are intermediate between those of linear polymers and hard colloids.[2,5,6] They consist of a number of arms or linear polymers f (also referred to as the functionality) covalently bonded at one end to a common centre. The degree of interpenetrability between adjacent stars is dependent on f as well as on the number of monomers associated with each arm. As $f \rightarrow 1$ or 2, their properties are similar to those of linear polymers while for $f \rightarrow \infty$, the particles tend towards sterically stabilized spherical colloidal particles, thus mimicking hard spheres with extensive excluded volume effects. The dynamics of star polymers is significantly different to that of linear polymers due to the presence of a single branch point which prevents reptation.[7,8] Rather, star dynamics are governed by the relaxation of the star arms by contour length fluctuations (CLF). CLF is an entropically unfavorable process and is exponentially dependent on the number of arm entanglements or constraints for well-entangled star arms.[9,10] Consequently star polymers can be viewed as soft colloids that bridge the behaviours of linear polymer chains and hard spheres.

The linear rheological response of star polymer melts is well known in that there are two separate relaxation processes; arm relaxation (polymeric), which is independent of f, and structural or centre of mass relaxation (core), which is a function of f and star polymer size.[6] However, like with many branched polymers the nonlinear flow behaviours of star polymers are less understood. Yet, a combination of experiments and computer simulations can provide deeper insight into the rheological responses of star polymers.

To properly characterise the long time response of dense star polymer systems requires a simulation approach capable of accessing extensive time and length scales. Coarse-grained models are ideally suited for this purpose where polymers are represented as a series of beads,[11–13] with each bead representing a group of monomers, or where each polymer is represented by a single point.[14] The latter case forms the basis of the Responsive Particle Dynamics (RaPiD) algorithm, a highly coarse-grained model which has been successfully applied to simulate a variety of linear and nonlinear fluid behaviours in solutions and melts.[15–19]

Recently a mean-field coarse-grained model where chains are represented as random walks of a particular step length has been applied to predict the nonlinear

[a)]Electronic addresses: barry.w.fitzgerald@gmail.com and b.fitzgerald@utwente.nl.

viscoelastic response of star melts with a small number of entangled arms, i.e., $f = 4$.[20] However, the RaPiD algorithm, with its particular coarse-grain approach, can serve as a bridge between polymers (low f) and colloids (high f) and additionally predict the response of both unentangled and entangled polymer systems. This combination underlines the strength of the RaPiD approach and is tested here with new experimental data on the linear and the nonlinear viscoelastic response of a polystyrene (PS) star melt. The PS stars have low M_a (below the entanglement limit and thus unentangled), moderate functionality, and are effectively monodisperse. For the simulations, we select an appropriate potential of mean force for star polymers and unlike in a previous RaPiD study on high f star polymers,[16] we account for distance dependent relaxation times between neighbouring stars.

There have been some experimental[21,22] and numerical[23,24] studies on unentangled or slightly entangled star polymer systems but the number of such studies is small in comparison to those for entangled star polymers. For example, experiments on moderate to high functionality unentangled star melts[21] show a viscoelastic response consistent with the Rouse-Zimm model[25] for unentangled polymer chains. In addition, previous studies have focused primarily on the linear viscoelastic response with little or no results on the nonlinear response of unentangled stars. In this study, through a combination of simulations and experiments, we address the shortfall of investigations on unentangled star melts by studying both their linear and nonlinear rheology.

This paper is arranged as follows. In Sec. II we present the star polymer sample used as well as the experimental measurements of the linear rheology. We then outline the RaPiD algorithm and the specifications made for the simulation of star polymer melts in Sec. III. We present a comparison of the linear rheology between experiments and simulations in Sec. IV where we find very satisfactory quantitative agreement. In Sec. V we study the response of the star polymer melts subject to a series of start-up shear protocols and the subsequent relaxation of shear stress upon the removal of shear. Finally we discuss the significance and perspectives of this work in Sec. VI.

II. EXPERIMENTS

A. Sample

Polystyrene star samples with $f = 16$ unentangled arms were anionically synthesized with a polydispersity index (PDI) < 1.1 and thus represent a well defined model polymer. The synthetic approach is the same as those used in Refs. 26 and 27. The molecular characteristics of the polymer are presented in Table I. The hydrodynamic radius R_h was estimated from light scattering experiments for star polymers in toluene, an athermal solvent. As an approximation we assume the arms do not significantly retract under melt conditions such that R_h remains effectively constant in the absence of solvent. This approximation is supported by previous experiments on linear PS polymers where a negligible change in R_h is observed for low M_w polymers in both solvents and melts.[28] Using R_h we calculate the overlap concentration c^* (see Table I). Using R_h we can also estimate both the radius of gyration R_g and the corona diameter σ_s. The corona diameter is the only relevant length scale for star polymers and represents the spatial extension of monomers on each arm from the central branching point as described by the Daoud-Cotton model.[29] As the arms of the PS stars are not extensively large, they may only satisfy the intermediate region of the density profile proposed in the Daoud-Cotton model.[29] Experiments on large functionality stars, i.e., $f \geq 64$ show that the ratio between the hydrodynamic radius and the radius of gyration is $R_h/R_g \approx 1.3$.[26] We apply this relationship as an approximation for the PS stars in

TABLE I. Molecular characteristics, set parameters and simulation parameters for the $f = 16$ polystyrene (PS) star polymer.

	Symbol	Value	Unit
Molecular characteristics			
Molecular weight per arm	M_a	13.2	kg/mol
Polydispersity Index	PDI ($=M_w/M_n$)	1.02	...
Hydrodynamic radius	R_h	9	nm
Radius of gyration	R_g	6.92	nm
Corona diameter	σ_s	9.23	nm
Overlap concentration	c*	329.16	kg/m^3
Mass density/concentration	c	1250 (3.8c*)	kg/m^3
Set parameters			
Number of particles	N	1250	...
Length of system cube side	L	71.92	nm
Temperature	T	403	K
Typical star-star distance (From CMA simulations)	r_{ij}^t	$0.75\sigma_s$	nm
Absolute number of constraints	n_0^a	2.0	...
Simulation parameters			
Entanglement number deviation	α	30	k_BT
Entanglement friction	ξ_e	$6 \cdot 10^{-6}$	kg/s
Maximum τ	τ_0	25	s
Decay length of τ	λ	0.15	σ_s

this study. We estimate σ_s using this expression and the relation $\sigma_s \approx \frac{4}{3} R_g$ which has been derived from simulations.[30]

B. Rheology

The linear viscoelastic response of the PS star polymer melt was measured experimentally using both frequency sweep (FS) and stress relaxation measurement approaches. First FS measurements were performed on a ARES 2kFRTN1 strain-controlled melt rheometer (TA Instruments) over a temperature range 110 °C–160 °C with a parallel plate geometry of 8 mm diameter. Temperature control was ±0.1 °C and all measurements were performed in a nitrogen environment to reduce the risk of degradation. The lower temperature limit is determined by the glass transition temperature of well entangled PS stars (approximately 100 °C) while the upper temperature limit is set by the final relaxation time of the sample as well as the accuracy of the transducer. Samples were subject to frequency sweeps consistent with small amplitude oscillatory shear (SAOS). Time-temperature superposition (TTS) was performed at a reference temperature $T_{ref} = 130$ °C and the Williams-Landel-Ferry model (WLF) were calculated in order to generate a master curve. Vertical shift factors were calculated from the density compensation: $b_T = \rho(T_{ref})(T_{ref} + 273.15)/(\rho(T)(T + 273.15))$ where $\rho(T) = 1250.3 - 0.605(273.15 + T)$ with ρ in kg/m^3.[31] On the other hand the horizontal shift factors a_T result from two-dimensional minimization whose variation is described by the WLF equation: $\log(a_T) = -C_1(T - T_{ref})/C_2 + T - T_{ref}$.[10] The WLF parameters were obtained by fitting the variation of a_T with the WLF equation. The horizontal and vertical shift factors for the PS stars are shown in Fig. 1. The data and WLF fits are consistent with other PS architectures and molar masses referred to the same temperature.[27,32]

At low frequencies in the FS measurements, large errors in the storage modulus G' can develop at high phase angles (approaching 90°) where the loss modulus G'' far exceeds G'. In this regime, only a small amount of the response signal is associated with G' and as such a slope characteristic of terminal relaxation for G' may be absent. To achieve better accuracy at low frequencies, we performed stress relaxation

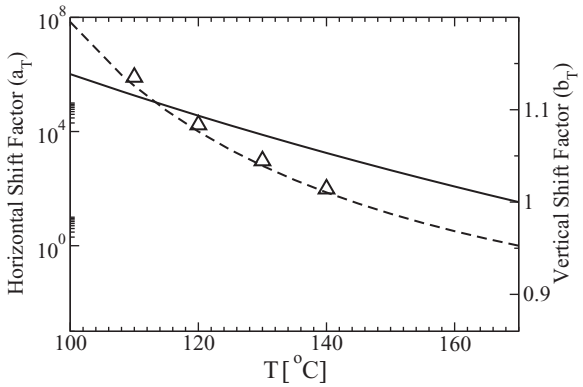

FIG. 1. WLF shift factors horizontal (symbols) and vertical (full line) for the PS star polymer superimposed with a WLF fit to the horizontal shift factors calculated for linear, star, ring, and H polymer PS samples[32] (dashed line). Shift factors for the PS star polymer melt were obtained between the range 110 °C and 140 °C. For the WLF fit: $C_1 = 5.6$, $C_2 = 120$, and $T_{ref} = 170$ °C.

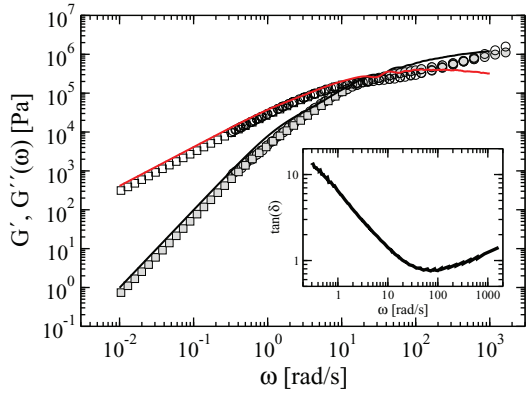

FIG. 2. Main figure: Storage ($G'(\omega)$) and loss ($G''(\omega)$) moduli for the $f = 16$ PS star polymer melt. The simulation data is represented by the solid lines ($G'(\omega)$ in black and $G''(\omega)$ in red) and obtained through the Fourier transform of $G(t)$ using Eq. (10) and Eq. (11). Moduli measured in experiments using frequency sweep (circles) and stress relaxation (squares) are also shown with the open symbols representing $G'(\omega)$ and the filled symbols $G''(\omega)$. Inset figure: tan of the phase angle δ as measured in experiments.

measurements in the linear regime. The stress relaxation measurements of samples were performed on a Anton Paar Physica MCR 501 stress-controlled rheometer with 8 mm parallel plates. A temperature control of ±0.1 °C was attained with a Peltier system in a nitrogen atmosphere. The conversion of $G(t)$ from stress relaxation to $G'(\omega)$ and $G''(\omega)$ was done with a commercial software package. The linear rheology for the PS star polymer melt from experiments are shown in Fig. 2. The stress relaxation measurements clearly resolve the terminal region thus alleviating any potential issues with measurements at low frequencies. The inset of Fig. 2 shows the variation of the tan of the phase angle, $\tan(\delta) = G''(\omega)/G'(\omega)$. For branched polymers the tangent of the phase angle can be more sensitive towards identifying specific relaxation processes.[32] For the PS star, the minimum in $\tan(\delta)$ is indicative of the onset of single branch point relaxation which continues for longer times.

For nonlinear measurements, the application of large, rapid shear deformations on polymeric systems in rotational rheometers leads to nonlinear flow instabilities such as melt fracture. Nonlinear start-up shear and subsequent steady state relaxation measurements were performed on the PS star for a large range of shear rates using a special cone-partitioned plate (CPP) equipped with temperature control.[33] The CPP apparatus consists of a 25 mm stainless steel cone with an angle of 0.1 rad, a stainless steel parallel plate 6 mm in diameter and a custom-built stainless steel partitioned plate with a gap of 0.15 mm. For further details see Ref. 33. A temperature control of ±0.1 °C was achieved with a home-made ceramic oven custom-made to fit around the CPP. The CPP setup delays edge fracture as only the central portion of the sample contributes to the measurement and thus it requires some time before the edge fracture propagates towards the sample center.

III. RAPID ALGORITHM

To simulate the dynamical properties of the PS star polymer melts we use the RaPiD algorithm[14,16,19] which is based upon a classical Brownian Dynamics approach. RaPiD has

been previously applied to study shear banding,[19] particle alignment in viscoelastic fluids,[34] highly entangled polymer melts,[15] nonlinear rheology,[17] and polymer chain diffusion.[35] In RaPiD, each fluid constituent, i.e., polymer, is coarse grained to a single particle whose position is described by just its centre of mass. The remaining degrees of freedom are used to account for an appropriate potential of mean force and transient pair-wise forces. It is the latter contribution that provides a viscoelastic description for particle interactions with the updated position of any particle being dependent on previous polymer conformations.

A. Potential of mean force

A potential of mean force suitable for star polymers has been derived using a scaling theory approach[36] and the Daoud-Cotton blob model for star polymer conformations.[29] This potential has been validated using small angle neutron scattering data from experiments[5] and Molecular Dynamics (MD) simulations.[30] The potential of mean force (or free energy) is approximated as a pairwise potential for stars that is valid for $f > 10$. In effect, the stars can be viewed as hybrid entities coupling a polymeric nature with the influence of a core region, where the latter is more prevalent for large f. In this study of moderate functionality PS stars ($f = 16$), the polymeric nature dominates albeit with some influence of a very small core region. Excluded volume effects are implicitly included in the potential. For two star polymers whose centres are separated by a distance r_{ij} the potential is expressed as

$$\beta V_{ss}(r_{ij}) = \frac{5}{18} f^{3/2} \begin{cases} -\ln\left(\frac{r_{ij}}{\sigma_s}\right) + \frac{1}{1+\psi} & r_{ij} \le \sigma_s \\ \frac{1}{1+\psi}\frac{\sigma_s}{r_{ij}} \exp(\psi - r_{ij}\kappa) & else \end{cases}, \tag{1}$$

where σ_s is the corona diameter, $\beta = (k_B T)^{-1}$, $\kappa = (2\sigma_s/\sqrt{f})^{-1}$, and $\psi = \sigma_s \kappa$. Here κ represents the decay length or the diameter of the outermost blobs of the star polymer arms as depicted in the Daoud-Cotton model.[29] For $r_{ij} \le \sigma_s$, the potential is that derived by Witten and Pincus[36] while for $r_{ij} > \sigma_s$, where interactions are due to a diffuse layer of fluctuating chains, the potential has a Yukawa form[37,38] whose amplitude is determined by the criterion of continuity at $r_{ij} = \sigma_s$. As for large r_{ij} the potential is effectively zero, we use a cutoff distance of $r_c = 3\sigma_s$ such that $V_{ss}(r > r_c) = 0$. Fig. 3 shows the ultra-soft nature of the star polymers for moderate functionality stars while a core effect manifests itself for $f = 128$. In the limit $f \to \infty$, the potential diverges for $r < \sigma_s$ while tending to zero for $r > \sigma_s$. Previous MD simulations[39] reveal that many-body forces for concentrations up to four or five times the overlap concentration are negligible. For the PS stars in this study we are within this regime where $c \approx 3.8c^*$. Therefore, it is appropriate to use the pairwise potential of mean force given by Eq. (1) in this study since many-body forces can safely be excluded.

B. Transient potential

Consider the same two star polymers we used in the definition of the potential of mean force. The stars find themselves in an equilibrium state with the centres separated by r_{ij} but with $r_{ij} < r_c$. In this state they have overlapped or interpenetrated leading to constraints due to interdigitation of the arms of the individual stars. For the PS star in this study $M_a < M_e$ where M_e is the entanglement mass. Thus rather than entangling neighbouring PS stars interpenetrate leading to the development of topological constraints. In the equilibrium state we denote the number of constraints for these stars as $n_0(r_{ij})$ while in general n_{ij} is the number of constraints between the stars when out of equilibrium. Once perturbed, a transient attractive potential Φ_t develops originating from a separation of time scales, namely, the relaxation time for the small scale polymer configuration and the time for the centres of mass to move an appreciable distance. This transient potential is described by a quadratic function,

$$\Phi_t = \frac{1}{2}\alpha(n_{ij} - n_0(r_{ij}))^2, \tag{2}$$

which has been introduced by van den Noort *et al.*[19] In effect Φ_t develops due to deviations of n_{ij} from $n_0(r_{ij})$ while α determines the allowed fluctuations in n_{ij}. Since α appears in the product $\alpha n_0(r_{ij})^2$ we fix the variation of one variable while using the other as a fitting parameter. Here we assume that $n_0(r_{ij})$ scales with the number of contacts between the arm monomers of neighbouring stars. In accordance with a previous approach for star polymer solutions[16] we use a Gaussian dependence for $n_0(r_{ij})$ such that

$$n_0(r_{ij}) = n_0^a \exp\left(-\frac{r_{ij}^2}{\sigma_s^2}\right), \tag{3}$$

where n_0^a is a prefactor which sets the absolute number of constraints. In simulations on $f = 128$ polybutadiene (PB) star polymer solutions, $n_0^a = 10$ was chosen such that $n_0(r_{ij}) \approx 1$ at the typical star-star distance r_{ij}^t.[16] Here we use results from cooperative motion algorithm (CMA) simulations[40,41] to estimate r_{ij}^t and then with Eq. (3) we calculate n_a^0 for the PS star polymer samples. These values are listed under "set parameters" in Table I. Having fixed the variation of $n_0(r_{ij})$ we only need tune α to determine the allowed fluctuations in the transient potential. For $r_{ij} > r_c$ we assume $n_0(r_{ij}) = 0$.

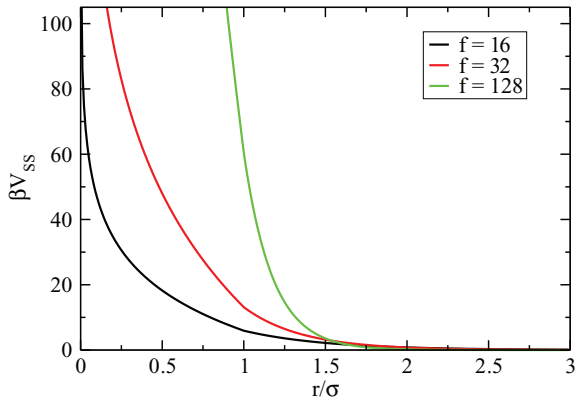

FIG. 3. Potential of mean force for star polymers with $f = 16$, 32, and 128. Note that inter-star distance r is scaled by the corona diameter, σ_s.

C. Propagator for particle motion

Particle positions are updated using a Brownian Dynamics propagator[19] which is derived from methods used to obtain the Smoluchowski equation.[42,43] Over the Smoluchowski time scale where the average velocity is zero, the displacement of a particle is given by

$$d\mathbf{r}_i = \frac{1}{\xi_i}\sum_j \left\{ -\frac{dV_{ss}}{dr_{ij}} + \alpha(n_{ij} - n_0(r_{ij}))\frac{dn_0}{dr_{ij}} \right\} \frac{\mathbf{r}_{ij}}{r_{ij}} dt + \nabla_i(k_B T/\xi_i)dt + \Theta_i\sqrt{2k_B T dt/\xi_i} + V(y)\hat{\mathbf{e}}dt, \quad (4)$$

where ξ_i is the particle-dependent friction parameter. In previous RaPiD approaches the friction was composed of the background solvent friction and the constraint friction. For the star polymer melts we need only consider the contribution from star polymer constraints such that ξ_i is given by

$$\xi_i = \xi_e \sum_j \sqrt{n_{ij} n_0(r_{ij})}, \quad (5)$$

where ξ_e is the friction per constraint; notice that its value depends on the normalization of $n_0(r_{ij})$. In Eq. (4) the first term accounts for the potential of mean force and transient potential. As the friction for any particle depends on the position of its neighbours (Eq. (5)), particle diffusion is not constant and must be corrected for by including the second term. The third term in Eq. (4) represents the Brownian motion of the particles where Θ_i is a time-dependent Markovian random vector of unit variance and zero mean, with three independent components and with no correlations across particles. The final term accounts for the average flow field due to an applied shear flow. Details for the calculation of $V(y)$ are presented at the end of this section.

Particle constraints undergo relaxation towards their respective equilibrium value $n_0(r_{ij})$ as described by

$$dn_{ij} = -\frac{1}{\tau}(n_{ij} - n_0(r_{ij}))dt + \Theta_{ij}\sqrt{\frac{2k_B T dt}{\alpha\tau}}, \quad (6)$$

where Θ_{ij} is a random number with unit variance, zero mean, and without correlations across particle pairs. The first term on the right hand side describes the rate at which n_{ij} approaches $n_0(r_{ij})$ subject to a characteristic relaxation time τ. The second term is a stochastic term describing Brownian fluctuations in the number of constraints which will persist even when $n_{ij} = n_0(r_{ij})$. As star separation decreases, constraints due to interdigitation between neighbouring stars increases and thus require longer times to relax. Hence a distance dependence for τ is included and given by

$$\tau(r_{ij}) = \tau_0 \exp\left(-\frac{r_{ij}}{\lambda}\right), \quad (7)$$

where τ_0 is a time constant and λ is the decay length for the relaxation time. Unlike the particle displacement propagator in Eq. (4), there is no spurious drift term in Eq. (6) since τ is independent of n_{ij}. That τ depends on r_{ij} (Eq. (7)) is not of relevance in this respect.

All simulations are carried out in a cubic box subject to periodic boundary conditions. Each initial configuration consists of 1250 particles distributed randomly throughout the system but subject to a maximum pair potential between neighbouring stars $\beta V_{ss}^m = 80\, k_B T$. The length of a cube side is a function of the mass density (1250 kg/m^3) and molecular weight of the star (fM_a). To study the nonlinear response of the star polymer melts, a shear flow is applied along the x-direction with a velocity gradient $\dot{\gamma}$ in the y-direction by using Lees-Edwards boundary conditions.[44] The equation of motion has been adapted to account for the inclusion of these boundary conditions. At every time step, the instantaneous flow field in the x-direction is calculated for a set of planes that are equally spaced on the y-axis by distributing the displacements of each particle to its two adjacent planes using a lever-rule. An average flow velocity $V(y)$ at time t is then calculated at each plane by averaging previous velocities at time t' with a weight function proportional to $\exp(-(t-t')/\tau)$ with $\tau = 10^{-3}$ s.

D. Comment on model parameters

The RaPiD algorithm is based upon a phenomenological description of polymers at the mesoscopic scale. Associated with this description are the transient potential parameters α, ξ_e, τ_0, and λ, as well as the equilibrium number of constraints $n_0(r_{ij})$ which have been introduced in Subsections III B and III C. A link between these RaPiD parameters and underlying polymer molecular characteristics may be provided through both simulation or theory. A recent study on low functionality star polymer melts has yielded these parameters from small scale simulation.[45] However, a theoretical prediction of these parameters will be the subject of a future study.

We now quickly review the influence of the polymer architecture on the parameters. First consider $n_0(r_{ij})$, the equilibrium number of constraints. Low f-high M_a star polymers represent open structures that can easily interpenetrate neighbouring stars, similar in effect to linear polymers. With increasing distance between stars $n_0(r_{ij})$ would be expected to quickly decay, possibly as a linear function. At the other extreme, high f stars with short arms (low M_a) are more compact objects similar to hard colloids.[46] Inside the corona radius of the object the monomer density is high and approximately linear with distance, while beyond the corona radius the monomer density has a Gaussian decay.[46] For these entities $n_0(r_{ij})$ can be approximated by a Gaussian function. For moderate f stars such as the PS stars in this study, $n_0(r_{ij})$ is approximated as a Gaussian function given that these stars would include the contribution of a small localised core region. The recent bottom-up approach mentioned above has been applied to low f star polymer melts to extract values for some of the transient parameters in RaPiD. The parameter α is related to the normalization of $n_0(r_{ij})$ and describes the resulting fluctuations in n_{ij} as given by Eq. (2). In small scale simulations, α was calculated from the variance in constraint numbers using equipartition theorem.[45] An estimate of τ_0 can be made from the crossing frequency of the experimental moduli. Inherent to many polymer systems, however, is a range of frequencies originating in some part from the polymer molecular characteristics. Therefore, the crossing frequency yields only an estimate of the dominant relaxation time. The parameter λ is linked to the magnitude of polymer overlap. For

large r_{ij} the degree of overlap between particles is small, and hence the decay to $n_0(r_{ij})$ will be faster than at small r_{ij}. Essentially, λ dictates how quickly the relaxation time of the n_{ij} decreases with increasing distance. Finally, the friction per polymer constraint ξ_e can be estimated by studying fluctuations in forces from small scale simulations.[47] However, measuring ξ_e using this approach requires a large data set due to the fast fluctuating interactions represented by both random forces and frictions.[47] In the small scale simulations of star polymer melts,[45] the authors instead adjusted ξ_e to tune the diffusion coefficient from RaPiD simulations to that from small scale simulations.

IV. SIMULATING LINEAR RHEOLOGY

A. Method

As outlined in Sec. III, each star polymer is subject to two potentials; a potential of mean force (Eq. (1)) and a transient potential (Eq. (2)). The potential of mean force, which determines the equilibrium structural properties, is a function of the molecular characteristics such as the corona diameter σ_s and functionality f. These parameters are listed in Table I. For the transient potential we have introduced a number of simulation parameters in Table I which are associated with the constraint dynamics. These parameters, α, ξ_e, τ_0, and λ, along with $n_0(r_{ij})$ account for the coupling between the dynamics of the eliminated and retained coordinates. These parameters are to be adjusted to match the experimental rheology as closely as possible.

In RaPiD one of the main observables is the shear relaxation modulus $G(t)$ which is calculated from the autocorrelation of the shear stress σ_{xy} using

$$G(t) = \beta V \langle \sigma_{xy}(t)\sigma_{xy}(0)\rangle, \tag{8}$$

where V is the volume of the simulation system. The shear stress is calculated according to the expression

$$\sigma_{xy}(t) = -\frac{1}{V}\sum_{i,j}(r_{i,x} - r_{j,x})F_{ij,y}, \tag{9}$$

where $F_{ij,y}$ is the y-component of the total force acting on particle i due to the presence of particle j, both from the potential of mean force and the transient force.

In experiments, the storage and loss moduli are the standard linear rheological measurements. These quantities are related to the shear relaxation modulus by

$$G'(\omega) = \omega\int_0^\infty \sin(\omega t)G(t)\mathrm{d}t, \tag{10}$$

$$G''(\omega) = \omega\int_0^\infty \cos(\omega t)G(t)\mathrm{d}t. \tag{11}$$

Thus by first calculating $G(t)$ we can estimate from simulations the experimental moduli. We obtain an estimate of $G(t)$ from the experimental moduli by approximating the moduli with a Generalised Maxwell model consisting of n modes in parallel over the entire experimental frequency range. The resulting $G(t)$ curve provides an approximation that can be used for a quick comparison of the experimental and simulation results during the fitting procedure. However, the final quality of the model should be judged on the comparison of $G'(\omega)$ and $G''(\omega)$. The values of the "simulation parameters" in Table I are estimated by using the approach presented in Ref. 17. First α is varied until we obtain good agreement in $G(t)$ at low times. The relaxation of $G(t)$ is then obtained by simultaneously varying τ_0 and λ. The tail of $G(t)$ is dependent on λ such that for decreasing λ the tail becomes less abrupt. Finally, we vary the constraint friction parameter ξ_e to adjust $G(t)$ to the correct time scale. We refer the reader to Ref. 17 for further details on this approach.

B. Recovering experimental moduli

In Fig. 2 we compare the storage and loss moduli calculated from simulations with measurements from experiments. The RaPiD parameters for the moduli are $\alpha = 30\ k_BT$, $\tau_0 = 25$ s, $\lambda = 0.15\ R_g$, and $\xi_e = 6 \times 10^{-6}$ kg/s. From experiments the response is consistent with that of the Rouse model, which is applicable to both unentangled linear[48] and star polymers[49] in solutions and melts, and is characterised by a number of relaxation modes. For $\omega < 1/\tau_R$, where τ_R is the longest or first relaxation mode for Rouse polymers (also the Rouse time), we find $G'(\omega) \propto \omega^2$ and $G''(\omega) \propto \omega$, consistent with the emergence of a terminal relaxation regime. For $\omega \geq 1/\tau_R$ or the higher Rouse mode, $G'(\omega)$ and $G''(\omega)$ are almost indistinguishable and parallel such that $G'(\omega) \simeq G''(\omega) \propto \omega^{0.5}$ which is consistent with observations for linear polymers and theoretical expectations for star polymers.[23,49] The simulations recover the terminal region for $\omega < 1/\tau_R$, while above $1/\tau_R$ we find good agreement between experiment and simulation up to $\omega \approx 100$ rad/s. Agreement is not expected in the high frequency range, i.e., $\omega > 100$ rad/s. The RaPiD model cannot adequately resolve this range as the model has coarse grained all local degrees of freedom corresponding to the high frequency response.

V. SHEAR PROTOCOLS

In Sec. IV we recovered the linear rheology of the PS star polymer melt and in the process found the RaPiD "simulation parameters." In this section we present results on start-up shear protocols and cessation or shut down and compare simulation output with experiment. All nonlinear shear experiments were undertaken at 130 °C, which is the reference temperature T_{ref} used to generate the TTS master curve as outlined in Sec. II.

A. Start-up shear stress

For a start-up shear protocol, samples are subject to a constant shear rate $\dot\gamma$ commencing at $t = 0$ s where $\dot\gamma = 0\ \mathrm{s}^{-1}$ for $t < 0$ s. Fig. 4 shows the start-up shear stress, σ^+, for different shear rates from experiments and simulations. For all shear rates simulations match the initial transient shear stress to at least approximately 0.08 s. Beyond this time the level of correspondence is dependent on the shear rate. At low shear rates ($\dot\gamma < 5.62\ \mathrm{s}^{-1}$), σ^+ first increases before

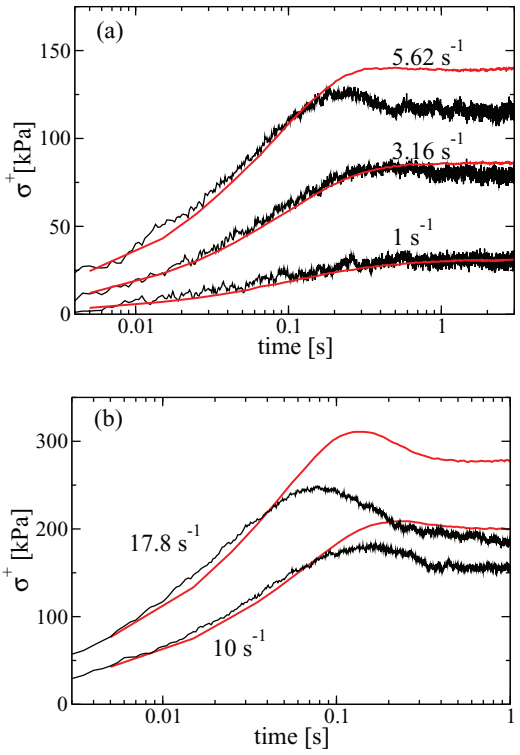

FIG. 4. Start-up shear stress σ^+ for the PS star polymer melt for a number of different applied shear rates $\dot{\gamma}$. The black curves represent the simulation data while the red curves come from experiments. Shear rates are indicated on the figures. Each simulation curve represents the ensemble average of 10 independent simulations.

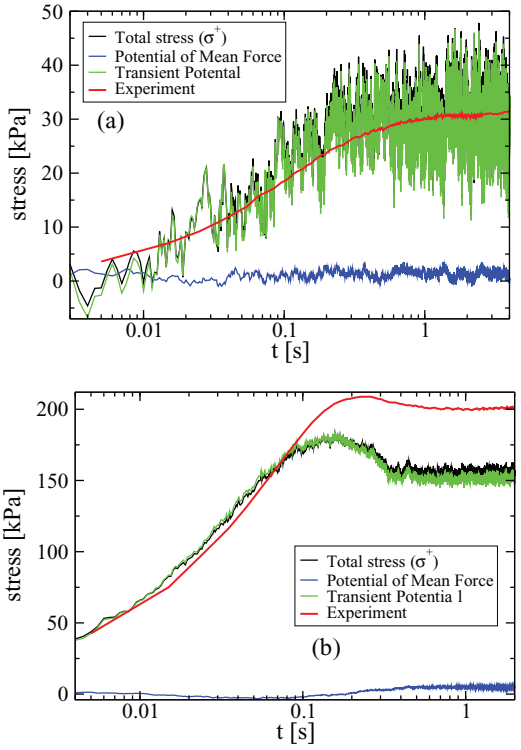

FIG. 5. Total stress $\sigma^+(t, \dot{\gamma})$ (black) separated into the contributions from the potential of mean force (blue) and the transient potential (green) for (a) $\dot{\gamma} = 1\ \mathrm{s}^{-1}$ and (b) $\dot{\gamma} = 10\ \mathrm{s}^{-1}$. Experimental data (red) is included in each plot. Each simulation curve represents the ensemble average of 10 independent simulations.

reaching a steady-state response after 0.5 s, an experimental behaviour recovered to good agreement by simulation (Fig. 4(a)). However, for $\dot{\gamma} = 5.62\ \mathrm{s}^{-1}$ simulations predict a stress overshoot at approximately 0.2 s with this feature absent experimentally. For $\dot{\gamma} = 10\ \mathrm{s}^{-1}$ and $17.8\ \mathrm{s}^{-1}$ (Fig. 4(b)), both experiments and simulations display an obvious stress overshoot although simulations underestimate both the magnitude of the overshoot and the steady-state response of the system. Simulations also predict that the overshoot occurs at a slightly earlier time than found experimentally. In the case $\dot{\gamma} = 17.8\ \mathrm{s}^{-1}$, there is significant disagreement with regards to the nature of the steady-state response. Due to sample size constraints in experiments, the stress response was measured for only 1 s at high shear rates by which time a steady-state response is evident.

In Fig. 5 we plot the total stress as well as the contributions arising from the potential of mean force V_{ss} and the transient potential Φ_t for $\dot{\gamma} = 1\ \mathrm{s}^{-1}$ and $\dot{\gamma} = 10\ \mathrm{s}^{-1}$. The stress contribution from the transient potential is strongly correlated with the total stress for both shear rates, an observation consistent with coarse-grained simulations of high-functionality star polymer solutions.[16] For $\dot{\gamma} = 1\ \mathrm{s}^{-1}$, where simulations agree with the experimental response, the total stress is almost entirely described by the transient potential with the potential of mean force only relevant at steady-state. At $\dot{\gamma} = 10\,\mathrm{s}^{-1}$ the qualitative features of a stress overshoot followed by a steady-state regime are recovered with simulations. An initial shear stress increase towards overshoot is accounted for by the stress contribution from the transient potential until $t \approx 0.1$ s after which quantitative differences become most prominent. These differences might be attributed to the absence of particle deformation in the particle description of the RaPiD model implemented here. We will comment on this further in relation to the nonlinear flow curves.

To construct nonlinear flow curves from the start-up shear response, we extracted both the maximum stress at overshoot σ_{max} and the steady state stress σ_{steady}. Using these measures we calculated the maximum shear viscosity as $\eta_{max} = \sigma_{max}/\dot{\gamma}$ and the steady-state shear viscosity as $\eta_{steady} = \sigma_{steady}/\dot{\gamma}$ for a number of shear rates. The flow curves are shown in the main figure of Fig. 6. For η_{steady}, the simulated shear viscosity qualitatively recovers the shear thinning behaviour of the melt. We find good correspondence at low shear rates, where shear thinning effects are small, while at higher shear rates where shearing effects are prominent the viscosity decays steeper than in experiments.

A scaling analysis theory for unentangled polymer melts predicts the emergence of shear thinning, which decreases by a power law with exponent −2/3, provided the finite extensibility of the polymer chains is considered explicitly.[51] In another theoretical approach based upon the Rouse model, the shear thinning regime declines with an exponent of −1/2 and is applicable to monodisperse unentangled polymer melts and polymer solutions[52]. From Fig. 6 the experimental decay is similar to the theoretical prediction, however the shear thinning curve from simulations differs from theory (with an exponent ≈−1.22). Direct comparison with theory is tentative as both theories[51,52] apply to linear polymer chains. With such

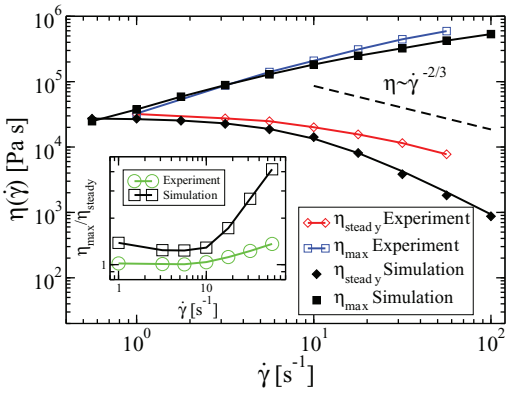

FIG. 6. Main figure: Comparison of viscosity measures, η_{steady} and η_{max}, from experiments and simulations for the $f = 16$ PS star polymer melt. Simulation results are represented in black (closed diamonds for η_{steady} and closed squares for η_{max}) while the experimental data are shown in colour. η_{steady} from simulations (closed diamonds) is fitted with the Cross model.[50] The remaining solid lines are included as guides for the eye. The dashed line is a scaling analysis prediction for unentangled polymers.[51] Inset: η_{max}/η_{steady} as a function $\dot{\gamma}$ for both experiments and simulations.

a decrease in the shear thinning curve, i.e., steeper than –1, we expect shear banding effects,[53] but this is not seen here during simulation. The absence of shear banding may be attributed to the finite size of the simulation box.[54]

This steeper decay in the viscosity is also reminiscent of RaPiD simulations on polymer solutions where the shear thinning behaviour, although recovered, was also too steep.[34] The faster shear thinning effect is related to the absence of polymer deformation that would facilitate particle elongation and subsequent re-emergence of constraints between particles in their neighbourhood. A recent variant of the RaPiD algorithm, where polymers may deform, has shown that for linear polymers both the linear and nonlinear rheology can be recovered when particle elongation is incorporated.[17] Here, we also qualitatively recover the trend of an increasing maximum viscosity which is indicative of an increasing stress overshoot with $\dot{\gamma}$. At the higher shear rates there is a slight underestimate from simulations for η_{max}.

The relationship between η_{max} and η_{steady} is shown in inset of Fig. 6. We note that the increase in η_{max}/η_{steady} occurs at the same rate, i.e., $\dot{\gamma} = 10\ s^{-1}$ where the onset of shear thinning becomes obvious. The slope of η_{max}/η_{steady} from $\dot{\gamma} = 10\ s^{-1}$ for the experimental data is very close to that observed for low functionality highly entangled polyisoprene (PI) star polymer melts.[27] The difference in the simulation data can be attributed as above for the steeper shear thinning to the absence of polymer deformation. We also calculated γ_{max} which is the strain where η_{max} for the shear thinning regimes. For $10\ s^{-1} \leq \dot{\gamma} \leq 60\ s^{-1}$, we found $2.4 < \gamma_{max} < 3$ for experiments, while for simulations $1.3 < \gamma_{max} < 1.5$. For linear polymers where stretching is absent, it has been predicted that $\gamma_{max} = 2.3$.[55] For the experimental data we are above this strain for all shear rates, thus suggesting polymer stretching is connected with the onset of shear thinning. However, the simulation data is below the prediction for linear polymers. This is a tentative comparison, however, since the PS stars here are of moderate f (distant from linear) and they consist of unentangled arms in contradiction to the entangled PI star melts.[27]

B. Cessation

To study the relaxation of stress from the steady state, σ^-, the applied shear was removed such that $\dot{\gamma} = 0\ s^{-1}$ at $t \geq 0$ s. In order to compare the relaxation process for different shear rates we normalised each time series with the initial stress state where $\sigma_{norm} = \sigma^-(t)/\sigma(t = 0)$. In Fig. 7(a) we plot the variation of σ_{norm} for different shear rates from simulations. We also include the relaxation of σ_{norm} as calculated for $G(t)$ from simulations for an equilibrium system, or the linear regime, using the expression

$$\sigma_{norm}(t) = 1 - \frac{\int_0^t dt' G(t')}{\int_0^\infty dt' G(t')}. \tag{12}$$

In effect this represents the relaxation of a system that prior to cessation was subject to infinitesimal shear. With the removal of shear the system approaches an equilibrium state. However, the relaxation for systems initially subject to shear is notably faster than for the equilibrium case. All curves are effectively relaxed after 1 s and for $\dot{\gamma} > 10\ s^{-1}$ the relaxation curves are almost indistinguishable. In Fig. 7(b) we show the variation of σ_{norm} from experiments for a subset of the shear rates presented in Fig. 7(a). Comparison of the curves shows that the simulations recover the qualitative form of the stress

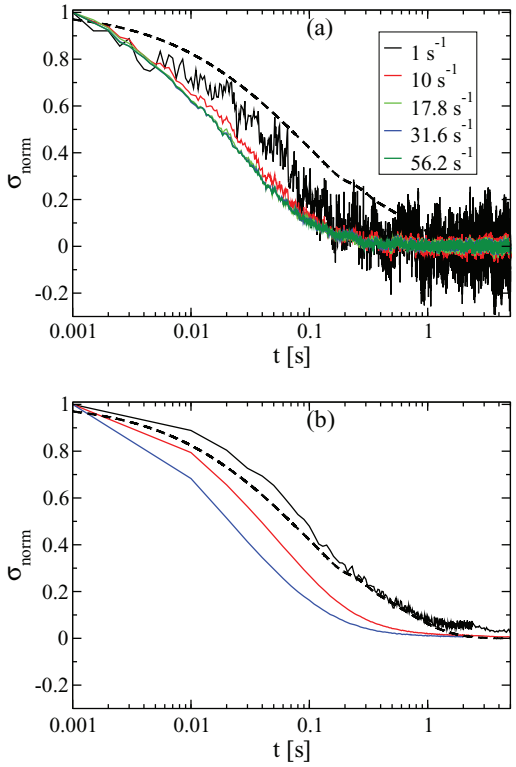

FIG. 7. The relaxation of the normalised shear stress σ_{norm} from simulations (a) and experiments (b) for a number of different shear rates. The dashed line in both figures represents σ_{norm} as calculated from G(t) from simulations using Eq. (12). t is the time after which the imposed shear rate was removed. Each simulation curve (in (a)) represents an ensemble average over 10 simulations.

relaxations for the real melt. Comparing with Fig. 7(a) we note that the relaxations for $\dot{\gamma} = 1\ s^{-1}$ in experiments are closer to the equilibrium relaxation curve (dashed line) than in the case of simulations. With increasing $\dot{\gamma}$ the difference between the experimental and simulation curves decreases. These results suggest that for the lower shear rates the simulations slightly overestimate the relaxation process.

VI. DISCUSSION AND CONCLUSIONS

In this paper we have presented results from experiments and highly-coarse grained simulations, using the RaPiD algorithm, on both the linear and nonlinear rheology of a moderate functionality PS star polymer melt. In RaPiD, each polymer entity is viewed as a single particle where all eliminated degrees of freedom are used to define a free energy and transient pair-wise potential. For star polymers, a free energy pair-wise function for high functionality stars is already available[5,29] while the transient potential used here is an improved version of a potential implemented for star polymer solutions.[16] The PS samples were anionically synthesized having a functionality $f = 16$ with a low molecular weight per arm of $M_a = 13.2$ kg/mol as well as being a well defined polymer with a very low polydispersity. RaPiD presumes all polymer fluids are perfectly monodisperse.

For the linear rheology, we have recovered, through simulation, the experimental moduli to good agreement. We also replicated the terminal response of the melt at low frequencies. Having identified the RaPiD "simulation parameters" (as listed in Table I) that reproduce the linear rheology, we then focused on the response of the PS star polymer melt to simple shear, and upon removal of shear, the ensuing relaxation. First we have simulated the qualitative features of a stress overshoot followed by a steady-state response at high shear rates. Best correspondence is found at low shear rates, where a stress overshoot is absent, and where agreement between experiments and simulations is excellent. However, with increasing shear rate, the RaPiD simulations underestimate both the peak in the overshoot and the steady-state response. These differences are summarised in the nonlinear flow curves (Fig. 6) where the steady-state and maximum viscosity from experiments are plotted. The overshoot behaviour from both experiments and simulations can also be presented in terms of the start-up viscosity η^+ with strain as in Fig. 8. In both experiments and simulations we see behaviours reminiscent of soft particles as opposed to hard colloids. For simulations (Fig. 8(a)), we observe the overshoot at $\gamma \approx 1.5$, which is a higher strain than for hard colloids where the overshoot peak develops below $\gamma = 1$.[56] From the experimental curves in Fig. 8(b) we notice that the overshoot peaks occur at $\gamma \gtrsim 2$, corroborating with recent experiments on low functionality polyisoprene star melts.[27] In RaPiD, overshoots occur when the flow brings the particles out of equilibrium, which takes at least one strain unit to occur. These curves serve as motivation for the inclusion of a description of particle deformation in subsequent simulations.

By applying a cessation or shut-down protocol we studied the relaxation process in systems that were initially subject to shear (Fig. 7). For shear rates where some degree of shear-

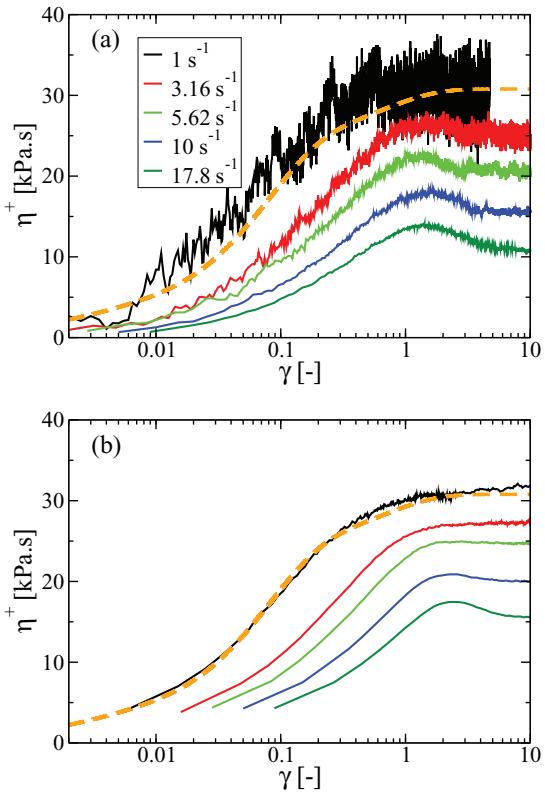

FIG. 8. Start-up viscosity $\eta^+ = \sigma^+/\dot{\gamma}$ plotted against strain γ for the PS star polymer melt from simulations (a) and experiments (b) for a number of different shear rates. Dashed line in both figures represents η^+ as calculated from G(t) from simulations using the expression $\eta^+(t) = \int_0^t dt' G(t - t')$. Each simulation curve (in (a)) represents an ensemble average over 10 simulations.

thinning is already observed, we find that stress relaxations are notably faster than those for systems in the linear regime. In addition, simulations recover the qualitative features of the relaxation process for all shear rates with the best agreement observed at higher shear rates (Fig. 7). Simulation results predict that the overshoot and the steady-state shear response are almost entirely associated with the transient potential (Fig. 5). In a previous study on high M_w, high functionality entangled star polymers solutions, the conservative potential (Eq. (1) in this paper) contributes an appreciable fraction of the steady-state response.[16] The small contribution of the conservative potential towards the steady-state shear stress for the star polymer melts in this study (Fig. 5) is consistent with the Rouse-like behaviour, i.e., entangled, of the star arms. Although entanglements are absent and stars are constrained through interpenetrating with their neighbours, the pair-wise conservative potential implemented here may underestimate equilibrium interactions. As such an adjustment to the conservative potential to account for many-particle interactions in the melt state may be used in a future study to improve upon the depiction of the equilibrium state and thus the respective contribution of the transient and conservative interactions towards the steady-state shear response.

Although we have found the shear-thinning behaviour of the real melt, we slightly overestimate the shear thinning effect at shear rates $\dot{\gamma} > 10\ s^{-1}$. We propose that this steeper shear thinning effect may be due to the absence of a

description of particle deformation in the model. RaPiD simulations of linear polymer solutions where such deformation is described have fully recovered the shear-thinning behaviour as well as the linear rheology.[17] For those simulations, each deformable particle consists of two coarse-grained particles or components that can both entangle with surrounding deformable particles. Deformability is captured by introducing a FENE (Finite-Extensible Non-Linear Elastic) potential which allows the distance between components to vary and also acts as a penalty for the free energy.

In this study we considered a PS star melt, far above the overlap concentration which may have repercussions for the degree of polymer deformation and resulting conformational changes when subject to shear. Recent studies have provided further insight into the conformational properties of star polymers, both entangled and unentangled, subject to shear. First, simulations using a coupled MD – multiparticle collision dynamics (MPCD) approach have shown that unentangled stars with large f in solutions of varying concentrations, both below and far above the overlap concentration, are less deformed and less aligned than low f star polymers.[57] A simple calculation based on the Rouse model for linear polymers, where the polymers can be viewed as stars with $f = 1, 2$, by Colby *et al.*[52] reveals that the shear thinning regime develops due to the stretching of the Rouse chains as they are perturbed by the shear flow. Although a Rouse model has been developed for star polymers,[23] it has yet to be employed to study the significance of particle deformation on the rheological response. Finally, experiments on highly entangled low functionality ($f < 10$), high M_a PI star polymer melts and solutions reveal orientation also plays an important role in the stress overshoot (in that particular case it clearly dominated over stretching).[27] In all cases, the degree of deformation and orientation would be moderated by the presence of a branching point and the degree of functionality of the stars. These findings from simulations and experiments provide further justification for need to include a description of particle deformation in a RaPiD model for star polymers.

In the current version of RaPiD it is also impossible to decipher the emergence of particle alignment as all particles are spherical whereas simulations with the deformable particles show that particle alignment is amplified at high shear rates for the case of linear polymers in solution.[17] Using deformable particles would differentiate between the importance of particle alignment and particle deformation towards the development of the stress overshoot in star polymer melts, as well as possibly correct for the steeper shear-thinning effect predicted by the current simulations. As a result this would demonstrate the universal prediction of the linear and nonlinear response for unentangled and entangled star polymers (all of which interpenetrate) using RaPiD.

ACKNOWLEDGMENTS

The authors acknowledge financial support from the EU through the FP7 European Soft Matter Infrastructure, ESMI Grant Agreement No. 262348. The authors gratefully acknowledge financial support from the Dynacop-network (FP7 ITN DYNACOP Grant No. 214627).

[1] D. Read, C. Das, J. den Doelder, M. Kapnistos, I. Vittorias, and T. McLeish, Science **333**, 1871 (2011).
[2] C. N. Likos, Soft Matter **2**, 478 (2006).
[3] X. Chen, M. Shahinur Rahman, H. Lee, J. Mays, T. Chang, and R. Larson, Macromolecules **44**, 7799 (2011).
[4] F. Snijkers, D. Vlassopoulos, H. Lee, J. Yang, T. Chang, P. Driva, and N. Hadjichristidis, J. Rheol. **57**, 1079 (2013).
[5] C. N. Likos, H. Löwen, M. Watzlawek, B. Abbas, O. Jucknischke, J. Allgaier, and D. Ritcher, Phys. Rev. Lett. **80**, 4450 (1998).
[6] D. Vlassopoulos, G. Fytas, T. Pakula, and J. Roovers, J. Phys.: Condens. Matter **13**, R855 (2001).
[7] M. Doi and S. F. Edwards, *The Theory of Polymers Dynamics* (Oxford Science Publications, Oxford, UK, 1986).
[8] P. de Gennes, J. Chem. Phys. **55**, 572 (1971).
[9] M. Doi, J. Polymer Sci., Polym. Lett. Ed. **19**, 265 (1981).
[10] J. Ferry, *Viscoelastic Properties of Polymers* (Wiley, New York, 1980).
[11] A. Clark, J. McCarty, and M. Guenza, J. Chem. Phys. **139**, 124906 (2013).
[12] L. Liu, J. Padding, W. den Otter, and W. Briels, J. Chem. Phys. **138**, 244912 (2013).
[13] G. Zhang, K. Daoulas, and K. Kremer, Macromol. Chem. Phys. **214**, 214 (2013).
[14] W. J. Briels, Soft Matter **5**, 4401 (2009).
[15] P. Kindt and W. J. Briels, J. Chem. Phys. **127**, 134901 (2007).
[16] J. T. Padding, E. van Ruymbeke, D. Vlassopoulos, and W. J. Briels, Rheol. Acta **49**, 473 (2010).
[17] I. S. Santos de Oliveria, B. W. Fitzgerald, W. K. den Otter, and W. J. Briels, J. Chem. Phys. **140**, 104903 (2014).
[18] A. van den Noort and W. J. Briels, J. Non-Newtonian Fluid Mech. **152**, 148 (2008).
[19] A. van den Noort, W. K. den Otter, and W. J. Briels, Europhys. Lett. **80**, 28003 (2007).
[20] M. Andreev, H. Feng, L. Yang, and J. Schieber, J. Rheol. **58**, 723 (2014).
[21] E. van Ruymbeke, E. B. Muliawan, D. Vlassopoulos, H. Gao, and K. Matyjaszewski, Eur. Polym. J. **47**, 746 (2011).
[22] N. Clarke, R. Colley, S. Collins, L. Hutchings, and R. Thompson, Macromolecules **39**, 1290 (2006).
[23] A. Ghosh and R. Colby, Polym. Prepr. **49**, 86 (2008).
[24] H. Watanabe, H. Yoshida, and T. Kotaka, Polym. J. **22**, 153 (1990).
[25] B. Zimm, J. Chem. Phys. **24**, 269 (1956).
[26] J. Roovers, L.-L. Zhou, P. Toporowski, M. van der Zwan, H. Iatrou, and N. Hadjichristidis, Macromolecules **26**, 4324 (1993).
[27] F. Snijkers, K. Ratkanthwar, D. Vlassopoulos, and N. Hadjichristidis, Macromolecules **46**, 5702 (2013).
[28] J. Cotton, D. Decker, H. Benoit, B. Farnoux, J. Higgins, G. Jannink, R. Ober, C. Picot, and J. des Cloizeaux, Macromolecules **7**, 863 (1974).
[29] M. Daoud and J. Cotton, J. Phys. (Paris) **43**, 531 (1982).
[30] A. Jusufi, M. Watzlawek, and H. Löwen, Macromolecules **32**, 4470 (1999).
[31] P. Zoller and D. Walsh, *Standard Pressure-Volume-Temperature Data for Polymers* (Technomic Publishing Co., New York, 1995).
[32] M. Kapnistos, D. Vlassopoulos, J. Roovers, and L. Leal, Macromolecules **38**, 7852 (2005).
[33] F. Snijkers and D. Vlassopoulos, J. Rheol. **55**, 1167 (2011).
[34] I. Santos de Oliveira, A. van den Noort, J. Padding, W. K. den Otter, and W. J. Briels, J. Chem. Phys. **135**, 104902 (2011).
[35] G. Schneider, K. Nusser, S. Neueder, M. Brodech, L. Willner, B. Farago, O. Holderer, W. Briels, and D. Richter, Soft Matter **9**, 4336 (2013).
[36] T. A. Witten and P. A. Pincus, Macromolecules **19**, 2509 (1986).
[37] H. Yukawa, Proc. Phys. Math. Soc. Jpn. **17**, 48 (1935).
[38] E. J. W. Verwey and J. T. G. Overbeek, *Theory of the Stability of Lyophobic Colloids* (Elsevier, New York, 1948).
[39] C. von Ferber, A. Jusufi, M. Watzlawek, C. Likos, and H. Löwen, Phys. Rev. E **62**, 6949 (2000).
[40] T. Pakula, Comp. Theor. Polym. Sci. **8**, 21 (1998).
[41] T. Pakula, D. Vlassopoulos, G. Fytas, and J. Roovers, Macromolecules **31**, 8931 (1998).
[42] P. Español and P. Warren, Europhys. Lett. **30**, 191 (1995).
[43] W. J. Briels, "Theory of polymer dynamics," Lecture notes (Uppsala University, 1994).
[44] M. Allen and D. Tildesley, *Computer Simulations of Liquids* (Clarendon, Oxford, 1987).
[45] L. Liu, W. den Otter, and W. Briels, "Coarse grain forces in star polymer melts," Soft Matter (published online 2014).
[46] F. Randisi and A. Pelisseto, J. Chem. Phys. **139**, 154902 (2013).

[47]J. T. Padding and W. J. Briels, J. Chem. Phys. **117**, 925 (2002).
[48]P. Rouse, J. Chem. Phys. **21**, 1272 (1953).
[49]M. Doi, Polym. J. **6**, 108 (1974).
[50]M. M. Cross, J. Colloid. Sci. **20**, 417 (1965).
[51]A. Subbotin, A. Semenov, E. Manias, G. Hadziioannou, and G. ten Brinke, Macromolecules **28**, 3898 (1995).
[52]R. H. Colby, D. C. Boris, W. E. Krause, and S. Dou, Rheol. Acta **46**, 569 (2007).
[53]J. K. G. Dhont and W. J. Briels, Rheol. Acta **47**, 257 (2008).
[54]J. K. G. Dhont, Phys. Rev. E **60**, 4534 (1999).
[55]M. Doi and S. F. Edwards, J. Chem. Soc., Faraday Trans. 2 **75**, 38 (1979).
[56]C. P. Amann, M. Siebenbürger, M. Krüger, F. Weysser, M. Ballauff, and M. Fuchs, J. Rheol. **57**, 149 (2013).
[57]S. Singh, D. Fedosov, A. Chatterji, R. Winkler, and G. Gompper, J. Phys.: Condens. Matter **24**, 464103 (2012).